ACS Catalysis

Research Article

pubs.acs.org/acscatalysis

# $MoS_2$ Nanosheets: A Designed Structure with High Active Site Density for the Hydrogen Evolution Reaction

Zhuangzhi Wu,[†,∥] Baizeng Fang,[‡,§] Zhiping Wang,[†] Changlong Wang,[†] Zhihong Liu,[∥] Fangyang Liu,[∥] Wei Wang,[⊥] Akram Alfantazi,[⊥] Dezhi Wang,*[,†] and David P. Wilkinson*[,‡,§]

[†]Key Laboratory of Ministry of Education for Non-Ferrous Materials Science and Engineering, School of Materials Science and Engineering, Central South University, Changsha 410083, China

[‡]Department of Chemical & Biological Engineering, University of British Columbia, 2360 East Mall, Vancouver, BC, Canada V6T 1Z3

[§]Clean Energy Research Center, 2360 East Mall, Vancouver, BC, Canada V6T 1Z3

[∥]School of Metallurgical Science and Engineering, Central South University, Changsha 410083, China

[⊥]Department of Materials Engineering, University of British Columbia, Vancouver, BC, Canada V6T 1Z4

Supporting Information

**ABSTRACT:** Two-dimensional $MoS_2$ nanosheets (NSs) with high active site density were designed for the hydrogen evolution reaction (HER) through a microdomain reaction method. The effect of the annealing temperature on the microstructure and the HER performance of $MoS_2$ NSs was examined, and a plausible relation between the stack structures of the $MoS_2$ catalysts and their HER performance was also explored. The $MoS_2$ NS electrocatalyst obtained at 550 °C reveals the best HER performance with a relatively small Tafel slope of 68 mV/dec. Both the exposed surface area and active site density are very important for providing a large amount of active sites. The present work has been proved to be an efficient route to achieve a high active site density and a relatively large surface area, which might have potential use in photoelectrocatalytic water splitting.

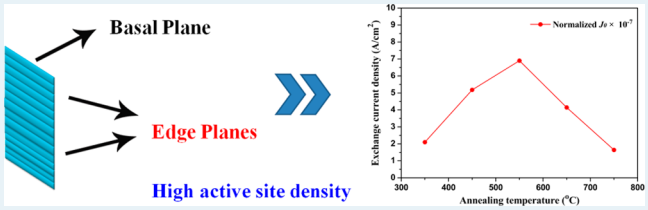


**KEYWORDS:** *molybdenum disulfide, nanosheets, active site density, electrocatalyst, hydrogen evolution reaction*

## 1. INTRODUCTION

Hydrogen energy is a clean resource and serves as one of the most promising candidates for replacing petroleum fuels in the future. Efficient hydrogen production is a core hurdle facing the development of a hydrogen based economy. Although platinum is well-known for its superior electrocatalytic property in the hydrogen evolution reaction (HER) in an acidic medium and commonly used as an electrocatalyst in this application,[1,2] large scale application of Pt is highly limited due to its high price and global low availability.[3−6] The development of an inexpensive, highly active, acid-stable HER electrocatalyst remains a major challenge.[7−9]

Recently, transitional metal sulfides such as nanometer-scaled $MoS_2$ and $WS_2$ have drawn great attention as inorganic electrocatalysts for HER due to their low cost, high chemical stability, and excellent electrocatalytic properties.[10−22] Three main techniques have been suggested to optimize the HER activity of $MoS_2$ and $WS_2$, including (1) increasing the catalytic activity of the active sites, (2) improving the electrical contact to these sites, and (3) increasing the number of active sites of the catalysts.[23] In order to increase the intrinsic activity of the active sites, some promoters were employed, such as Ni, Co, B, etc., which were widely studied in the hydro-treating catalysts of petroleum.[24−30] A recent report also demonstrated that the addition of cobalt could greatly enhance the electrocatalytic activity of $MoS_2$, due to a reduction of hydrogen binding energy from 0.18 to 0.10 eV, which is close to the 0.08 eV for the Mo edge.[11] As a result of doping with Co, all the edges become active for the HER. However, it must be noted that only 25% of the edge atoms are hydrogen covered during the reaction according to the density functional theory (DFT) calculation of hydrogen binding free energy, implying that only a fraction of the $MoS_2$ entities are active for the HER.[10,19] In order to improve the electrical contact to the active sites, some supports with excellent electrical conductivity have been investigated. Generally, carbon materials are commonly used as electrocatalyst supports for the HER and other electrochemical applications, mainly including carbon nanotubes,[23] macroporus-meosporous carbon materials,[31−35] graphene,[16] reduced graphene oxide sheets,[36] and so on.

As to the last point, there are two strategies to increase the number of active sites. The first one is to increase the surface area of catalysts or their supports for more exposed planes. However, the catalytic activity of $MoS_2$ has been reported not

Received: February 18, 2013
Revised: July 21, 2013
Published: July 29, 2013

  

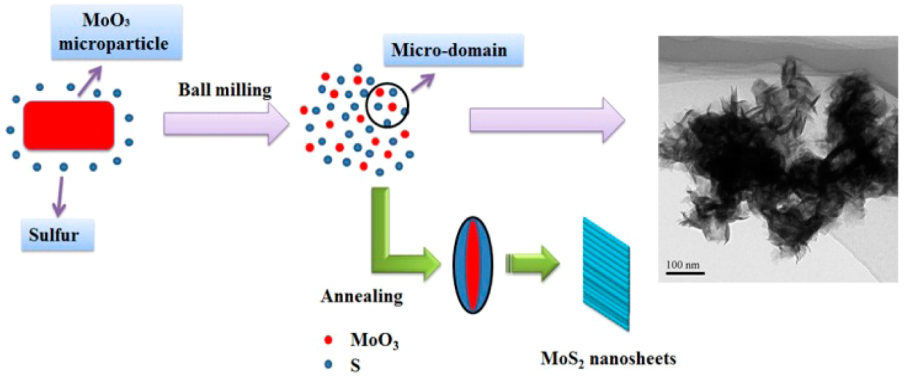


**Figure 1.** Schematic illustration of the synthesis procedure and structural model of $MoS_2$NSs.

to be proportional to the surface area, because the HER active centers for $MoS_2$ have been identified to be the edges of the hexagonal lamellar $MoS_2$ crystal layers, specifically the (10−10) edges,[10,19] and the basal planes have been found generally inert for the HER. If a great fraction of the high surface area was attributed to the exposure of basal planes, the total activity would not be greatly improved. Therefore, an intrinsic improvement in the density of active sites is much more important than a simple increase in the surface area, which requires a large ratio of perimeter-to-basal area (i.e., with more edge sites).

To meet this requirement, a great deal of effort has been devoted to modifying the surface structures of $MoS_2$ materials, including gentle oxidation of $MoS_2$,[37−39] functional structural design,[40,41] and stabilizing the edge layers with organic molecules.[13,21,42] However, most of these reports only presented low-stacked $MoS_2$ structures, resulting in a relatively low edge/basal ratio. To gain a maximum value of edge/basal ratio, a higher stack height (along *c* axis) with more edge sites and a smaller size of basal plane are required.

In this study, an optimized and tailored structure of $MoS_2$ nanosheets (NSs) has been developed by a microdomain reaction[43,44] and explored as a highly active catalyst for the HER. The tailored $MoS_2$ NSs catalyst possesses rich exposed edge sites with a thickness of only ca. 2 nm, achieving a higher value of the edge/basal ratio. Different from the previous reports[13,21,40−42] on $MoS_2$ with poor crystallinity and low stack heights, the current work demonstrates $MoS_2$ NSs with better crystallinity and higher stack layers. Moreover, the relation between the stack structures and the functions for the HER was also examined. Due to their tailored nanostructures with high active site densities, $MoS_2$ NS electrocatalysts, especially the one obtained at 550 °C, have demonstrated excellent HER performance.

## 2. EXPERIMENTAL SECTION

**2.1. Catalyst Synthesis.** The $MoS_2$ NSs catalysts were prepared by mechanical activation of $MoO_3$ and S microparticles, which creates microdomain effects and consequently produces NSs. Generally, gaseous and aqueous reactants more easily form nanoparticles due to closer contact of the reactants and faster reaction rates, while the solid-state reaction always produces large microparticles because of the low reaction rate resulting from the slow diffusion from the outer layer to the inner layer, resulting in the growth of crystal size. To limit the crystal growth and then produce nanoparticles by a solid-state route, we proposed a mechanical activation method, in which the reactants $MoO_3$ and S microparticles were ball-milled to get nanosized powder and close contact, forming a relatively isolated microdomain for sulfurization during the subsequent annealing process. Due to the mechanical activation, the ball-milled reactants could finish the sulfurization very quickly (within 10 min), and as a result the outer sulfurized layer could limit the growth of the inner oxide core and diminish the agglomeration of the as-obtained NSs at low temperatures. The synthesis procedure and structure mode for the fabrication of $MoS_2$ NSs is illustrated in Figure 1.

In a typical synthesis, 5 g of $MoO_3$ was mixed with 10 g of S and milled at room temperature in Ar for 24 h using a planetary ball mill. The mill operated at 400 rpm using stainless steel balls with a ball-to-powder ratio of 60:1 (w/w). The ball-milled mixture was subsequently annealed at a temperature varied from 350 to 750 °C for 60 min in a flow of Ar. The as-obtained $MoS_2$ catalysts were labeled as NSs-ttt, where ttt is the annealing temperature in °C.

**2.2. Physical Characterization.** X-ray powder diffraction (XRD) patterns for the various electrocatalysts were recorded using a D/max-2500 system with Cu K$\alpha$ radiation ($\lambda$ = 0.154 nm). Crystallite sizes were estimated from the diffraction patterns using the Scherrer equation. Microstructures were observed by scanning electron microscopy (SEM, FEI Sirion 200) and transmission electron microscopy (TEM, TecnaiG$^2$ 20). Specific surface areas were determined by $N_2$ adsorption at 77 K using a volumetric unit (Quadrasorb SI-3MP).

**2.3. Electrochemical Characterization.** To evaluate the electrochemical activities toward HER for various electrocatalysts, linear sweep voltammetry (LSV) measurements were conducted in 0.5 M $H_2SO_4$ in a three-electrode electrochemical cell with a scan rate of 2 mV/s on a IM6ex (Zahner, Gemany) at room temperature. An electrocatalyst deposited onto a glassy carbon disk was used as the working electrode. A detailed preparation procedure for the working electrode is presented as follows: 4 mg of the catalyst and 80 $\mu$L of Nafion solution (5 wt %) were dispersed in 1 mL of the mixed solution of deionized water and ethanol (4:1 in volume ratio). After ultrasonication for 30 min, 5 $\mu$L of the catalyst slurry was dropped onto the top of a glassy carbon disk. The obtained catalyst-coated glassy carbon was then dried at room temperature to yield a catalyst loading of 285 $\mu$g cm$^{-2}$. A saturated calomel electrode (SCE) was employed as the reference electrode and a Pt foil as the counter electrode. Prior to any electrochemical measurement, the electrolyte solution was purged with $N_2$ for 1 h to remove completely the oxygen, and stable polarization performance curves were recorded after 10 cycles. Electrode potentials were


dx.doi.org/10.1021/cs400384h | ACS Catal. 2013, 3, 2101−2107

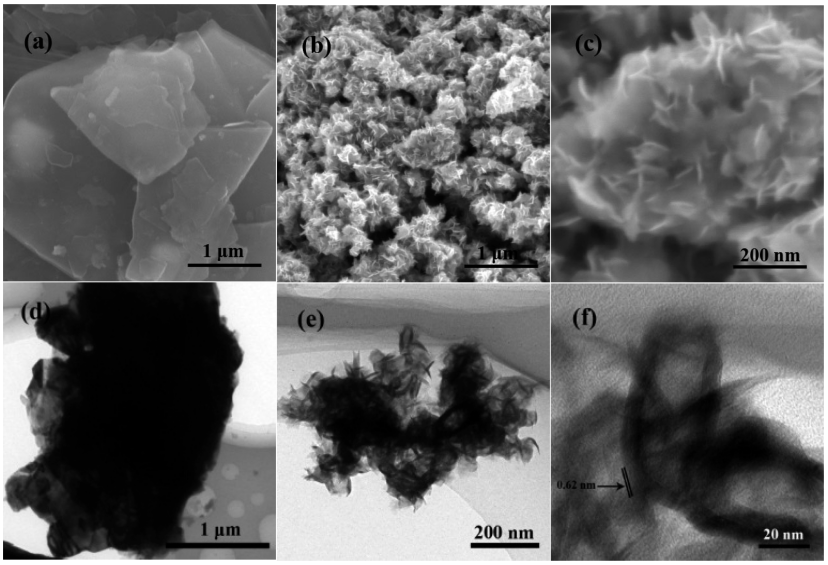


**Figure 2.** SEM (a, b, c) and TEM (d, e, f) images of the bulk C-$MoS_2$ microparticles (a and d) and typical $MoS_2$ NSs-550 (b, c, e, and f) .

recorded vs SCE reference electrode, which was calibrated with respect to reversible hydrogen electrode (RHE). The calibration was performed in an electrolyte saturated by high purity $H_2$ with a Pt wire as the working electrode, as reported by Li et al.[16] All the potentials reported in our manuscript are against RHE. In 0.5 M $H_2SO_4$, $E$(RHE) = $E$(SCE) + 0.273 V.

A commercial bulk $MoS_2$, marked as C-$MoS_2$, was purchased from Xilong Chemical Company, China, for the comparison of the HER performance of the various $MoS_2$-based catalysts.

## 3. RESULTS AND DISCUSSION

**3.1. Structure Characterization of $MoS_2$ NSs.** The $MoS_2$ NSs catalysts were synthesized via a microdomain reaction method[43,44] by ball-milling the mixture of $MoO_3$ and S, followed by annealing at high temperatures. Different stack heights were controlled by adopting different annealing temperatures. Due to similar structures of these catalyst samples, only the $MoS_2$ NSs sample obtained at 550 °C was selected to represent their typical morphologies and structures, which are shown in Figure 2. Compared to the bulk commercial $MoS_2$ microparticles (i.e., C-$MoS_2$) with large basal planes (Figure 2a), the $MoS_2$ NSs sample shows much smaller size and exposes more edge planes, as shown in Figure 2b. It was observed that all the NSs are less than 100 nm in size from a SEM image with a higher magnification (i.e., Figure 2c).

Further insight into the microstructures was obtained through the TEM images. One can see that the bulk C-$MoS_2$ (Figure 2d) is very large with size over 2 $\mu$m, consistent with the previous SEM observation. In contrast, as shown in Figure 2e and f, the NSs are much smaller with a length of about 100 nm and a width of about 10 nm. Although the thickness of the NSs cannot be determined from the present images because of the favorite orientation of lamellar $MoS_2$ on the copper grid, it can be estimated to be about 2 nm from our previous report,[43] in which the thickness was observed occasionally from the side of twisted NSs. Therefore, the present NSs are supposed to have a pretty high edge/basal ratio of 10 nm/2 nm, equal to 5:1. Moreover, the distance between two interlayers was also measured and shows a typical value about 0.62 nm, a little larger than the standard one with a tiny lattice expansion due to the curvature of interlayers.[45] Due to the similarity of the microstructures among the NSs samples obtained at different temperatures, as shown in Figure S1 in the Supporting Information, only the TEM images of NSs-550 were selected to compare with those of the C-$MoS_2$ in Figure 2. However, it must be noted that the increased temperatures improve the crystallinity of the NSs samples, resulting in higher stacking lamellar structures, consistent with the XRD analyses, as discussed below.

XRD patterns of the $MoS_2$ NSs obtained at different annealing temperatures (350−750 °C) are shown in Figure 3.

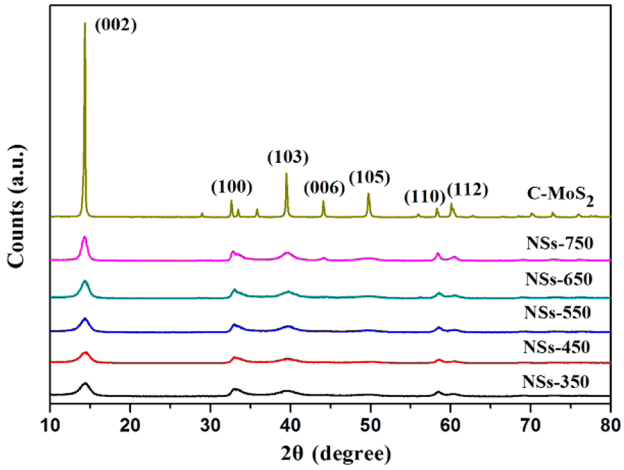


**Figure 3.** XRD patterns of $MoS_2$ NSs obtained at different annealing temperatures and bulk C-$MoS_2$.

All of these NSs can be indexed to the pure hexagonal $MoS_2$ (JCPDS card no: 65−0160). The prominence of the (002) peak indicates the presence of a well-stacked layered structures. With the increase of annealing temperatures, all of the reflection peaks are strengthened, indicating that the crystallinity is improved and the stack height is increased. Especially at 750 °C, the (006) and (112) peaks also become noticeable. The stack height along the $c$ axis of these samples was estimated from the diffraction patterns using the Scherrer equation and was listed in Table 1 along with their BET surface areas.


dx.doi.org/10.1021/cs400384h | ACS Catal. 2013, 3, 2101−2107

**Table 1. Stack Height and BET Surface Areas of Various Catalysts**

| sample | annealing temperature (°C) | stack height (nm) | interlayer numbers | BET surface area ($m^2/g$) |
|---|---|---|---|---|
| C-$MoS_2$ | | 47.6 | 76.8 | 4.0 |
| NSs-350 | 350 | 5.6 | 9 | 61.4 |
| NSs-450 | 450 | 5.8 | 9.4 | 58.3 |
| NSs-550 | 550 | 6.5 | 10.4 | 56.4 |
| NSs-650 | 650 | 7.1 | 11.4 | 35.0 |
| NSs-750 | 750 | 9.8 | 15.7 | 30.5 |

It is obvious that all the NSs prepared with the microdomain reaction method show much lower stack height and higher BET surface areas than the bulk C-$MoS_2$. And with the increase of annealing temperatures, the stack height of NSs is increased gradually because of the improvement of crystallinity. However, on the contrary, the BET surface areas drop down gradually because higher temperatures promote the crystal growth and reduce pore structures. It must be noted that there is a sharp reduction in BET surface area at 650 °C, which probably will affect the final function. Considering the BET surface area and stack height information together, it can be concluded that the bulk C-$MoS_2$ will show poor catalytic ability for HER, because it possesses a small surface area and a terrible edge/basal ratio (47.6 nm/several $\mu$m), only exposing a few available edge sites. And a higher activity is expected for these NSs because of their relatively higher surface areas and, more importantly, their engineered stack structures with higher edge/basal ratios.

**3.2. Electrocatalytic Activity toward HER.** The polarization curves of all the samples measured in 0.5 M $H_2SO_4$ with a scan rate of 2 mV/s at room temperature are shown in Figure 4. For comparison, bulk C-$MoS_2$ and bare glassy carbon (GC) were also included. As we know, $MoS_2$ is a poor HER catalyst in its bulk form,[19] and there is only a slight current density observed for the bulk C-$MoS_2$ catalyst in Figure 4. However, nanoparticulate $MoS_2$ is a more promising system, and DFT calculations have indicated that the edges of $MoS_2$ nanoparticles are active for HER.[10] As a result, excellent catalytic activity is expected for the designed $MoS_2$ NSs with more exposed edge sites. As shown in Figure 4, all the $MoS_2$ NSs exhibit much better activity than the bulk C-$MoS_2$, providing direct evidence for the previous DFT calculations.[10] Especially, the NSs-550 shows the best HER activity with a current density of 4.56 mA/$cm^2$ at −150 mV, which is ca. 228 times larger than that of bulk C-$MoS_2$ (i.e., 0.02 mA/$cm^2$). Moreover, the various NSs samples also show quite different catalytic activities, which are decided by their intrinsic structures. With the increase of annealing temperatures, the HER activity of NSs is increased first and reaches the maximum value at 550 °C, then drops down sharply afterward. NSs-750 shows the worst catalytic activity among these NSs catalysts with a current density of 0.14 mA/$cm^2$ at −150 mV but is still better than the bulk C-$MoS_2$.

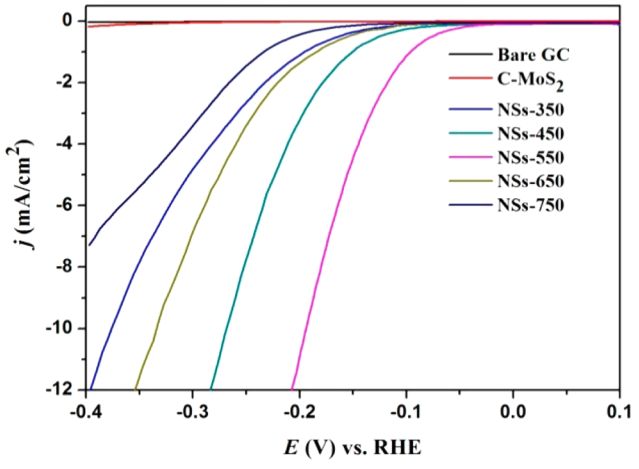


**Figure 4.** Polarization curves obtained in 0.5 M $H_2SO_4$ for various electrocatalysts.

The Tafel plots of these $MoS_2$ NSs derived from the polarization curves shown in Figure 4 fit well with the Tafel equation at different overpotential ranges, and only the linear portions were selected to give a clear comparison, as shown in Figure 5. Much smaller than that (i.e., 184 mV/dec) of the bulk C-$MoS_2$, the Tafel slopes of all the NSs catalysts are between 68 and 104 mV/dec, comparable with that of the previous reports.[11,47] A smaller Tafel slope means a faster increase of HER rate with the increasing potential.[15] Therefore, the NSs-550 still displays the best activity with the smallest slope value of 68 mV/dec.

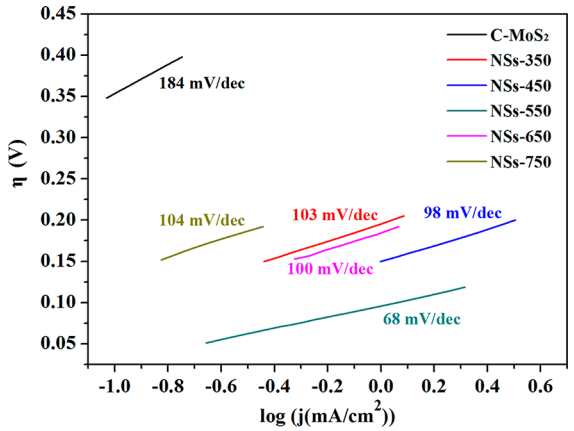


**Figure 5.** Tafel plots of various electrocatalysts.

Although the Tafel slope alone is insufficient to determine the specific mechanism of the HER, it does match the most recent report for molybdenum sulfide electrocatalysts assembled on a Au electrode.[46] More importantly and significantly, the current synthesis route is much easier and cheaper without using any noble metals.

Stability is another concern for the HER catalysts. To evaluate the HER stability of the NSs catalysts, long-term potential cycling stability of the NSs-550 catalyst was conducted by taking a potential scan from −0.3 to 0.1 V at a scan rate of 2 mV/s after 1000 cycles at an accelerated scanning rate of 100 mV/s. As shown in Figure 6, only a slight activity loss was observed after 1000 cycles, indicating a good durability.

The most inherent measure of activity for the HER is the exchange current density, $j_0$,[48−50] which is determined by fitting $j$-$E$ data to the Tafel equation.[48] The exchange current densities of all the samples are listed in Table 2. One can see that the C-$MoS_2$ reveals a $j_0$ of $3.0 \times 10^{-7}$ A/$cm^2$, which is comparable to that reported for C-$MoS_2$ materials in the previous studies,[19,22]


dx.doi.org/10.1021/cs400384h | ACS Catal. 2013, 3, 2101−2107

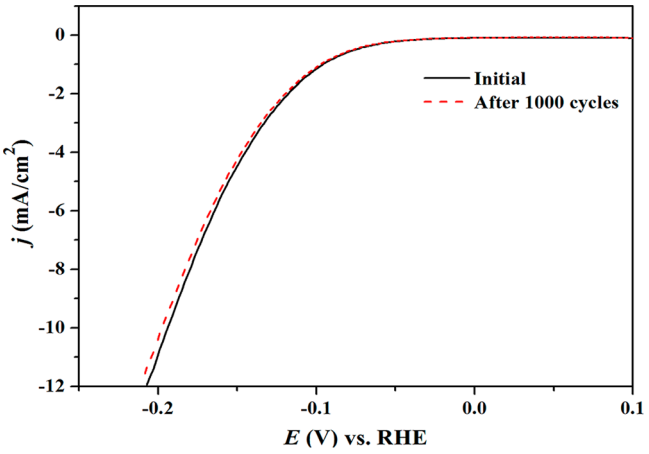


**Figure 6.** Stability test for the NSs-550 catalyst.

**Table 2. Tafel Slopes, Exchange Current Densities $j_0$, Normalized $j_0$, and Turnover Frequencies (TOFs) for Various $MoS_2$ Catalysts**

| sample | Tafel slope (mV/dec) | $j_0$ ($\times 10^{-5}$ A/cm$^2$) | normalized $j_0$ ($\times 10^{-7}$ A/cm$^2_{BET}$) | TOF[a] ($s^{-1}$) |
|---|---|---|---|---|
| C-$MoS_2$ | 184 | 0.03 | 0.75 | 0.001 |
| NSs-350 | 103 | 1.29 | 2.10 | 0.03 |
| NSs-450 | 98 | 3.02 | 5.18 | 0.06 |
| NSs-550 | 68 | 3.89 | 6.90 | 0.08 |
| NSs-650 | 100 | 1.45 | 4.14 | 0.03 |
| NSs-750 | 104 | 0.5 | 1.64 | 0.01 |

[a]The TOF here is actually defined as the per atom exchange rate of Mo.

while all the NSs catalysts show much larger values of $j_0$ by 1 or even 2 orders of magnitude. And the most active catalyst is NSs-550 with a largest $j_0$ of $3.89 \times 10^{-5}$ A/cm$^2$, which is about 130 times that of the bulk C-$MoS_2$. Considering that the NSs catalysts possess much higher surface area which can provide more exposed active sites, the $j_0$ data were normalized by BET surface area to give a fair comparison. It is obvious that the normalized exchange current density of NSs-550 is still 9.2 times larger than that of bulk C-$MoS_2$, which should be attributed to its high active site density.

It is well-known that the turnover frequencies (TOFs) of active edge sites should be the same without the addition of other promoters, and the activity is determined by the exposed edge active sites on the condition that the basal planes are inert. The BET surface area of $MoS_2$ catalysts includes the exposed inert basal planes and the active edge planes, playing an important role in all the catalytic reactions. Generally, larger BET surface area means more exposed active sites, guaranteeing higher activity. However, the catalytic activity is not always proportional with the BET surface area, because the incremental surface area could be contributed by the inert basal planes, providing no active sites for catalytic reactions, which was also proved in hydrotreating reactions.[49] In the present work, although the BET surface areas decrease with the increase in annealing temperatures, the activity is first improved and reaches the maximum value at 550 °C, then drops down afterward. $j_0$ and normalized $j_0$ also follow the same trend, as depicted in Table 2. Therefore, it can be concluded that the difference of normalized $j_0$ in Table 2 is caused by various active site densities, which can be described as the ratio of edge plane surface area/total surface area.

To get a direct site-to-site comparison, the TOFs ($s^{-1}$) of each site were also calculated following Jaramillo's method,[19] as shown in Table 2. It must be noted that the so-called sites here include inert basal and active edge sites, and the so-called TOF was actually defined as the per atom exchange rate of Mo, where the active sites were probably located. Despite a very low TOF value of C-$MoS_2$, the TOFs of the $MoS_2$ NSs catalysts are the same order of magnitude with the $MoS_2$ nanocatalyst (0.02 $s^{-1}$),[19] and the NSs-550 shows a highest TOF value of 0.08 $s^{-1}$, indeed in the high range of TOFs for metals. The obvious variation of TOF values among the various NSs catalysts are also attributed to the different active site densities. A higher active site density can enhance the TOF per site on average.

A summary of the exchange current densities ($j_0$) and Tafel slopes of various molybdenum sulfide catalysts investigated in the previous reports is shown in Table 3. One can see that the

**Table 3. A Summary of the Exchange Current Densities ($j_0$) and Tafel Slopes Reported for Various Molybdenum Sulfide Catalysts**

| catalyst | catalyst loading/ $\mu$g cm$^{-2}$ | $j_0$/A cm$^{-2}_{geometric}$ | Tafel slope/ mV dec$^{-1}$ |
|---|---|---|---|
| $MoS_2$ on Au (111)[19] | | $3.1 \times 10^{-7}$ | 55–60 |
| $MoS_2$[11] | | $4.6 \times 10^{-6}$ | 120 |
| $MoS_x$[47] | | | 53–65 |
| $MoS_2$ on carbon nanospheres[31] | 190 | | 41 |
| $MoS_2$ on RGO/free $MoS_2$[16] | 285 | | 41/94 |
| $MoS_2$/MWCNT[23] | | $4.0 \times 10^{-6}$ | 109 |
| $MoO_3$–$MoS_2$ nanowires[40] | | | 50–60 |
| $MoS_2$ on Au[46] | | $9.3 \times 10^{-6}$ | 69 |
| $MoS_2$[41] | | | 50 |
| $MoS_2$[51] | 8.5 | $2.2 \times 10^{-6}$ | 105–120 |
| NSs-550 | 285 | $3.89 \times 10^{-5}$ | 68 |

in-house NSs-550 catalyst shows much larger exchange current density and a relatively lower Tafel slope without any additives. It can be inferred that there are more exposed edge planes in the NSs-550 catalyst due to a higher edge/basal ratio, providing more active sites, which can generate a larger current at low overpotentials. With the introduction of highly conductive materials (Au, graphene, MWCNT, etc.), the HER activity can be greatly improved. Moreover, the amorphous $MoS_x$ also show excellent activity due to their quite different microstructures.

**3.3. The Relation between the Structure and HER Function.** It is widely accepted that the predominant active sites of $MoS_2$ are metallic edge planes with sulfur vacancies, whereas the basal plane, normally with completely coordinated sulfur atoms, is basically inert.[52,53] High-resolution scanning tunneling microscopy studies and theoretical calculations performed on nanoparticulate $MoS_2$ structures formed under sulfiding conditions implicated the formation of disulfide linkages or triangular $MoS_2$ units along the fully sulfide catalytically active edges of the layered structures, but the precise action modes of these sites remains elusive.[54,55] To identify the active edge sites of $MoS_2$ nanocatalysts for HER,


dx.doi.org/10.1021/cs400384h | ACS Catal. 2013, 3, 2101–2107

Jaramillo et al.[19] prepared $MoS_2$ nanoparticles with different sizes in an ultrahigh vacuum and confirmed that the edge site was indeed the active site, and the rate of reaction was directly proportional to the number of edge sites regardless of particle size. More importantly, they also proposed that changing the annealing temperature can control the ratio of basal planes to edge sites.[19]

Generally, higher activity can be achieved by enlarging the exposed surface area and enhancing the active site density. For bulk C-$MoS_2$, the exposed surface area is much lower than the NSs samples, and hence only a tiny $j_0$ is obtained with a value of $3.0 \times 10^{-7}$ A/cm$^2$. Eliminating the effect of surface area, the normalized $j_0$ gives a clearer insight into the origin of active sites. Although so, the bulk C-$MoS_2$ still exhibits the smallest normalized $j_0$. Therefore, the more dominant factor should be the active site density. For C-$MoS_2$, the stack height is only about 47.6 nm (Table 1), while the length or diameter of the basal plane is up to several micrometers (observed from the SEM and TEM images in Figure 2), resulting in a much smaller active site density. Due to the unique synthesis strategy, the $MoS_2$ NSs catalysts possess larger BET surface areas and higher active site densities with more active edge sites, and accordingly higher catalytic activity.

However, the microstructures of $MoS_2$ NSs, especially the exposed edge sites, are also strongly influenced by the annealing temperatures, resulting in various HER functions. To clarify this relation, in Figure 7 we plot the normalized $j_0$ versus the

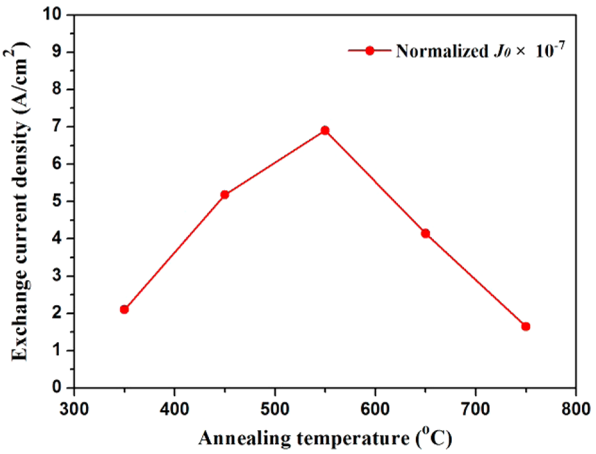


**Figure 7.** Normalized exchange current density versus the annealing temperature.

annealing temperature, which decides the stack height and BET surface area. With the increase of the annealing temperature from 350 to 550 °C, there are only slight increases and decreases in the stack height and BET surface area (as evident in Table 1), respectively. As evident from Figure 7, the normalized $j_0$ is enhanced with the increased annealing temperature associated with higher stack heights, approaching a maximum value of $6.90 \times 10^{-7}$ A/cm$^2$ at 550 °C. When annealed at 650 °C, the high annealing temperature not only accelerates the sulfurization (completed in less than 10 min[44]) but also promotes the agglomeration of NSs to form bulk basal planes, resulting in a sharp drop in BET surface area by 40% (Table[1]). When up to 750 °C, a sharp increase of the stack height from 11.4 to 15.7 layers is also observed, indicating a fast growth of crystal size with agglomerated basal planes. As a result, a smallest active site density is obtained, leading to the minimum normalized $j_0$ value of $1.64 \times 10^{-7}$ A/cm$^2$ at 750 °C.

**3.4. Further Improvements.** Although the $MoS_2$ NSs catalysts provide high active density, there is still a lot of room available to further improve their electrocatalytic activity. First, to enhance the inherent activity of each active site, Co can be adopted as a promoter,[11,15] as used in the hydrotreating catalysts of CoMoS.[56,57] Second, to improve the exposed surface area, porous structures with large surface area are preferred. Third, to minimize electronic transfer limitations, highly conductive supports are required. Therefore, to design a highly active HER catalyst to replace Pt, Co-promoted $MoS_2$ NSs coated on a porous support (such as graphene) with large surface area and excellent electronic conductivity are very promising candidates and this work is in progress.

Although it is widely accepted that the Mo atoms are likely the main active centers on the exposed edges,[10,19,51,54,55] based on some recent research reports, the rich S edges could play an important role in enhancing the HER activity,[14,17,46] and hence, it would be a very interesting and significant work to further investigate the effects from the sulfur edges, which is supposed to help us design $MoS_2$ materials with tailored nanostructures and improved HER performance, and this investigation is also in progress.

## 4. CONCLUSIONS

$MoS_2$ NSs catalysts with high active site density have been successfully synthesized with a microdomain reaction method, exhibiting excellent catalytic activity for the HER, and the active site density can be readily tailored by simply changing the annealing temperature. The highest active site density is observed at an annealing temperature of 550 °C over the catalyst NSs-550. Moreover, NSs-550 is the most active catalyst in the present work with a Tafel slope of 68 mV per decade. The excellent HER performance is due to the large amount of active sites, which are attributed to the high active site density and the relatively large exposed surface area. With the increase of the annealing temperature, the BET surface area and stack height decreases and increases, respectively, resulting in an increase of activity before 550 °C and a reverse drop after that. The present work gives a new method to engineer the lamellar structure of $MoS_2$ to expose more catalytically active edge sites, enabling improved performance. Further improvements of the activity can potentially be achieved by doping Co onto the edge sites of $MoS_2$ to form the highly active CoMoS phase followed by coating it onto a porous support with large surface area and high electronic conductivity.

## ■ ASSOCIATED CONTENT

### Supporting Information

HRTEM images for the samples annealed at different temperatures. This information is available free of charge via the Internet at http://pubs.acs.org.

## ■ AUTHOR INFORMATION

### Corresponding Author

*Phone: +86-731-88877221. E-mail: dzwang@mail.csu.edu.cn (D.W.), dwilkinson@chbe.ubc.ca (D.W.).

### Notes

The authors declare no competing financial interest.

## ■ ACKNOWLEDGMENTS

This work was supported by the Postdoctoral Science Foundation of China (2013M531801).

## ■ REFERENCES

(1) Raimondi, F.; Scherer, G. G.; Kotz, R.; Wokaun, A. *Angew. Chem., Int. Ed.* **2005**, *44* (15), 2190−2209.
(2) Tolle, R.; Otto, A. *Surf. Sci.* **2005**, *597* (1−3), 110−118.
(3) Arenz, M.; Stamenkovic, V.; Schmidt, T. J.; Wandelt, K.; Ross, P. N.; Markovic, N. M. *Surf. Sci.* **2002**, *506* (3), 287−296.
(4) Fang, B.; Kim, J.; Yu, J.-S. *Electrochem. Commun.* **2008**, *10* (4), 659−662.
(5) Fang, B.; Kim, M.; Kim, J.; Song, M.; Wang, Y.; Wang, H.; Wilkinson, D.; Yu, J.-S. *J. Mater. Chem.* **2011**, *21* (22), 8066−8073.
(6) Elezovic, N. R.; Gajic-Krstajic, L.; Radmilovic, V.; Vracar, L.; Krstajic, N. V. *Electrochim. Acta* **2009**, *54* (4), 1375−1382.1.
(7) Walter, M. G.; Warren, E. L.; Mckone, J. R.; Boettcher, S. W.; Mi, Q. X.; Santori, E. A.; Lewis, N. S. *Chem. Rev.* **2010**, *110* (11), 6446−6473.
(8) Li, Y.; Somorjai, G. A. *Nano Lett.* **2010**, *10* (7), 2289−2295.
(9) Hou, Y. D.; Abrams, B. L.; Vesborg, P. C. K.; Bjorketun, M. E.; Herbst, K.; Bech, L.; Stti, A. M.; Damsgaard, C. D.; Pedersen, T.; Hansen, O.; Rossmeisl, J.; Dahl, S.; Norskov, J. K.; Chorkendorff, I. *Nat. Mater.* **2011**, *10*, 434−438.
(10) Hinnemann, B.; Moses, P. G.; Bonde, J.; Jørgensen, K. P.; Nielsen, J. H.; Horch, S.; Chorkendorff, I.; Norskov, J. K. *J. Am. Chem. Soc.* **2005**, *127* (15), 5308−5309.
(11) Bonde, J.; Moses, P. G.; Jaramillo, T. F.; Nørskov, J. K.; Chorkendoff, I. *Faraday Discuss.* **2009**, *140* (0), 219−231.
(12) Tran, P. D.; Nguyen, M.; Pramana, S. S.; Bhattacharjee, A.; Chiam, S. Y.; Fize, J.; Field, M. J.; Artero, V.; Wong, L. H.; Loo, J.; Barber, J. *Energy Environ. Sci.* **2012**, *5* (10), 8912−8916.
(13) Karunadasa, H. I.; Montalvo, E.; Sun, Y.; Majda, M.; Long, J. R.; Chang, C. J. *Science* **2012**, *335*, 698−702.
(14) Vrubel, H.; Merki, D.; Hu, X. *Energy Environ. Sci.* **2012**, *5* (3), 6136−6144.
(15) Merki, D.; Hu, X. *Energy Environ. Sci.* **2011**, *4* (10), 3878−3888.
(16) Li, Y.; Wang, H.; Xie, L.; Liang, Y.; Hong, G.; Dai, H. *J. Am. Chem. Soc.* **2011**, *133* (19), 7296−7299.
(17) Merki, D.; Fierro, S.; Brubel, H.; Lu, X. *Chem. Sci.* **2011**, *2* (7), 1262−1267.
(18) Merki, D.; Vrubel, H.; Rovelli, L.; Fierro, S.; Hu, X. *Chem. Sci.* **2012**, *3* (8), 2515−2525.
(19) Jaramillo, T. F.; Jørgensen, K. P.; Bonde, J.; Nielsen, J. H.; Horch, S.; Chorkendorff, I. *Science* **2007**, *317*, 100−102.
(20) Wirth, S.; Harnisch, F.; Weinmann, M.; Schroder, U. *Appl. Catal., B* **2012**, *126*, 225−230.
(21) Lau, V. W.; Masters, A. F.; Bond, A. M.; Maschmeyer, T. *ChemCatChem.* **2011**, *3* (11), 1739−1742.
(22) Wu, Z.; Fang, B.; Bonakdarpour, A.; Sun, A.; Wilkinson, D. P.; Wang, D. *Appl. Catal., B* **2012**, *125*, 59−66.
(23) Laursen, A. B.; Kegnas, S.; Dahl, S.; Chorkendorff, I. *Energy Environ. Sci.* **2012**, *5* (2), 5577−5591.
(24) Yoosuk, B.; Kim, J. H.; Song, C.; Ngamcharussrivichai, C.; Prasassarakich, P. *Catal. Today* **2008**, *130* (1), 14−23.
(25) Alvarez, L.; Berhault, G.; Alonso-Nunez, G. *Catal. Lett.* **2008**, *125* (1−2), 35−45.
(26) Zhou, T.; Yin, H.; Liu, Y.; Chai, Y.; Zhang, J.; Liu, C. *Catal. Lett.* **2010**, *134* (3−4), 343−350.
(27) Wang, H.; Prins, R. *J. Catal.* **2009**, *267* (2), 193−201.
(28) Liu, B.; Chai, Y.; Liu, Y.; Wang, Y.; Liu, Y.; Liu, C. *Fuel* **2012**, *95*, 457−463.
(29) Okamato, Y.; Hioka, K.; Arakawa, K.; Fujikawa, T.; Ebihara, T.; Kubota, T. *J. Catal.* **2009**, *268* (1), 49−59.
(30) Usman; Kubota, T.; Araki, Y.; Ishida, K.; Okamoto, Y. *J. Catal.* **2004**, *227* (2), 523−529.
(31) Bian, X.; Zhu, J.; Liao, L.; Scanlon, M. D.; Ge, P.; Ji, C.; Girault, H. H.; Liu, B. *Electrochem. Commun.* **2012**, *22*, 128−132.
(32) Fang, B.; Chaudhari, N.; Kim, M.; Kim, J.; Yu, J. S. *J. Am. Chem. Soc.* **2009**, *131* (42), 15330−15338.
(33) Fang, B.; Kim, J.; Kim, M.; Yu, J. S. *Acc. Chem. Res.* **2013**, *46* (7), 1397−1406.
(34) Fang, B.; Kim, J.; Kim, M.; Bonakdarpour, A.; Lam, A.; Wilkinson, D. P.; Yu, J.-S. *J. Mater. Chem.* **2012**, *22* (36), 19031−19038.
(35) Kim, J.; Fang, B.; Song, M.; Yu, J. S. *Chem. Mater.* **2012**, *24* (12), 2256−2264.
(36) Firmiano, E. G. S.; Cordeiro, M. A. L.; Rabelo, A. C.; Dalmaschio, C. J.; Pinheiro, A. N.; Pereira, E. C.; Leite, E. R. *Chem. Commun.* **2012**, *48* (62), 7687−7689.
(37) Kautek, W.; Gerischer, H. *Surf. Sci.* **1982**, *119* (1), 46−60.
(38) Bahl, O. P.; Evans, E. L.; Thomas, J. M. *Proc. R. Soc. London, Ser. A* **1968**, *306* (1484), 53−65.
(39) Chianelli, R. R.; Ruppert, A. F.; Behal, S. K.; Kear, B. H.; Wold, A.; Kershaw, R. *J. Catal.* **1985**, *92* (1), 56−63.
(40) Chen, Z.; Cummins, D.; Reinecke, B. N.; Clark, E.; Sunkara, M. K.; Jaramillo, T. F. *Nano Lett.* **2011**, *11* (10), 4168−4175.
(41) Kibsgaard, J.; Chen, Z.; Reinecke, B. N.; Jaramillo, T. F. *Nat. Mater.* **2012**, *11*, 963−969.
(42) Lau, V. W.; Master, A. F.; Bond, A. M.; Maschmeyer, T. *Chem.—Eur. J.* **2012**, *18* (26), 8230−8239.
(43) Wu, Z.; Wang, D.; Sun, A. *J. Cryst. Growth* **2010**, *312* (2), 340−343.
(44) Wu, Z.; Wang, D.; Wang, Y.; Sun, A. *Adv. Eng. Mater.* **2010**, *12* (6), 534−538.
(45) Tenne, R.; Margulis, L.; Genut, M.; Hodes, G. *Nature* **1992**, *360* (6403), 444−446.
(46) Wang, T.; Liu, L.; Zhu, Z.; Papakonstantinou, P.; Hu, J.; Liu, H.; Li, M. *Energy Environ. Sci.* **2013**, *6*, 625−633.
(47) Benck, J. D.; Chen, Z.; Kuritzky, L. Y.; Forman, A. J.; Jaramillo, T. F. *ACS Catal.* **2012**, *2* (9), 1916−1923.
(48) Bockris, J. O. M.; Khan, S. U. M. *Surface Electrochemistry: A Molecular Level Approach*; Plenum: New York, 1993.
(49) Conway, B. E.; Tilak, B. V. *Electrochim. Acta* **2002**, *47* (22−23), 3571−3594.
(50) Norskov, J. K.; Bligaard, T.; Logadottir, A.; Kitchin, J. R.; Chen, J. G.; Pandelov, S.; Stimming, U. *J. Electrochem. Soc.* **2005**, *152* (3), J23−J26.
(51) Kong, D.; Wang, H.; Cha, J.; Pasta, M.; Koski, K.; Yao, J.; Cui, Y. *Nano Lett.* **2013**, *13* (3), 1341−1347.
(52) Roxlo, C. B.; Daage, M.; Ruppert, A. F.; Chianelli, R. R. *J. Catal.* **1986**, *100* (1), 176−184.
(53) Daage, M.; Chianelli, R. R. *J. Catal.* **1994**, *149* (2), 414−427.
(54) Lauristen, J. V.; Kibsgaard, J.; Helveg, S.; Topsoe, H.; Clausen, B. S.; Laegsgaard, E.; Besenbacher, F. *Nat. Nanotechnol.* **2007**, *2*, 53−58.
(55) Hansen, L. P.; Ramasse, Q. M.; Kisielowski, C.; Brorson, M.; Johnson, E.; Topsoe, H.; Helveg, S. *Angew. Chem., Int. Ed.* **2011**, *50* (43), 10153−10156.
(56) Okamoto, Y.; Kato, A.; Usman, S. K.; Hiromitsu, I.; Kubota, T. *J. Catal.* **2005**, *233* (1), 16−25.
(57) Huirache-Acuna, R.; Albiter, M. A.; Ornelas, C.; Paraguay-Delgado, F.; Martinez-Sanchez, R.; Alonso-Nunez, G. *Appl. Catal., A* **2006**, *308*, 134−142.